Hyperfine splitting of hydrogenlike thallium

M. Tomaselli,[1,2] T. Kühl,[2] W. Nörtershäuser,[2,3] S. Borneis,[2] A. Dax,[2] D. Marx,[2] H. Wang,[2] and S. Fritzsche[4]
[1]*Institute of Nuclear Physics, Darmstadt University, D-64289 Darmstadt, Germany*
[2]*GSI Gesellschaft für Schwerionenforschung, D-64291 Darmstadt, Germany*
[3]*Institute of Physics, Tübingen University, D-72076 Tübingen, Germany*
[4]*Institute of Physics, Kassel University, D-34132 Kassel, Germany*
(Received 5 February 2001; revised manuscript received 27 June 2001; published 4 January 2002)

The dynamic correlation model was used to calculate nuclear ground-state wave functions of ^{203}Tl, ^{205}Tl, and ^{207}Tl. The ground states of these isotopes are characterized by strong mixing amplitudes of the valence $3s_{1/2}^{-1}$ hole with the intrinsic vacuum states (valence hole coupled to core excitations). Nuclear magnetic moments, radii, and the 1*s* hyperfine-structure splitting energy for the hydrogenlike ions were calculated. Experimental magnetic moments and radii of the nuclear ground states are well reproduced. The hyperfine-structure splitting of the hydrogenlike Tl isotopes have not been measured so far, hence, the obtained values are only compared with predictions of other theoretical calculations. The difference in the 1*s* hyperfine-structure splitting between ^{203}Tl^{80+} and ^{205}Tl^{80+} is found to be 0.026 eV, which corresponds to a 3.1 nm shift in the transiton wavelength.

DOI: 10.1103/PhysRevA.65.022502 PACS number(s): 32.10.Fn, 21.60.−n, 21.10.Ky, 27.80.+w

I. INTRODUCTION

Hydrogenlike high-*Z* atoms offer fascinating possibilities for testing the interplay of nuclear and atomic structure. They have recently become available for experiments at GSI in Darmstadt [1,2] and at the LLNL in Livermore [3–5] and have been used to test the theory of quantum electrodynamics (QED) in extremely strong electric and magnetic fields [6]. Measuring the ground-state hyperfine structure (HFS) of these hydrogenlike systems is a sensitive method to explore QED and nuclear contributions to the electron energy. Experiments at GSI included laser spectroscopic investigations of ^{209}Bi^{82+} and ^{207}Pb^{81+} at the heavy-ion storage ring [1,2]. These measurements, with a relative accuracy better than 10^{-3}, allowed the first test of QED in the strong electromagnetic field of highly charged heavy ions. At Livermore, hydrogenlike ^{165}Ho^{66+} [4], ^{185}Re^{74+}, and ^{187}Re^{74+} [5] have been produced and stored in a high-energy electron-beam ion trap (SuperEBIT [3]) by an energy variable electron beam, axially compressed by a strong magnetic field. In this case, the HFS splitting was measured by passive photon-emission spectroscopy. Similar experiments are presently under preparation to measure the HFS of thallium isotopes [7].

For a theoretical determination of the HFS splitting both must be taken into account, nuclear structure as well as QED contributions. The dynamic correlation model (DCM) [8] was previously applied to ions in the region of the closed-shell nucleus ^{208}Pb to derive the nuclear part in the HFS. The DCM describes the structure of open-shell nuclei with an odd number of valence particles in terms of clusters: the valence and the core cluster. In contrast to Hartree-Fock approaches the DCM includes a coupling mechanism acting between the core and the valence particles, which modifies the Hartree-Fock description and polarizes the core via particle-hole excitations ($2\hbar\omega$) of protons and neutrons. Thus, the valence particle becomes ''dressed'' in the sense that it coexists with complex excitations of the core. From a Hartree-Fock (HF) point of view, these dressed particles correspond at most to a particular solution of an extended, nonlinear HF Hamiltonian. Pairing correlations are considered in the calculation of complex *n*-body matrix elements, even though they are not directly included in the model.

Previously reported DCM calculations showed good agreement with experimental data [1,2,4,5]. However, adding QED corrections to the DCM results led to a systematic deviation between theory and experiment [9,10]. Due to the uncertainty of the nuclear magnetic moments, especially for ^{207}Pb, where two different experimental values exist in literature, the good agreement between the DCM and the experiments was still unsatisfactory in understanding the role played by QED. In order to clarify this open point an analysis of the nonlinear terms contributing to the HFS was provided by performing a term-to-term comparison with the results of other theoretical models [11,12]. This was presented in [10], but it was not possible to get a solution for the important question concerning the interplay between nuclear and QED contributions. Moreover, up to now it is still unclear whether the larger splitting postulated by the DCM calculations with respect to other theories have to be associated with the Bohr-Weisskopf effect [13]. They could also be generated by relativistic nuclear effects [14], implicitly considered in this model. In the latter case, they have to be treated as additional contributions and could lead to a double-counting effect if the same terms appear in the QED corrections. This open point has motivated the application of the DCM to calculate the HFS of the hydrogenlike ^{203,205,207}Tl^{80+} ions, which is presented here. Besides, these calculations may guide future experiments at the GSI storage ring since an accurate *a priori* knowledge of the HFS transition frequency is required to avoid prohibitively large scan ranges.

In this work we present the results of DCM calculations for the thallium isotopes ^{203,205,207}Tl. The mixed-mode states were formed by coupling the single $3s_{1/2}^{-1}$ proton-hole to intrinsic core states with energies up to 30 MeV, classified in terms of configuration-mixing wave functions (CMWFs). We

found a strong admixture of particle-hole excitations to the single-particle states. These polarization states have a collective structure. They are formed by numerous particle-hole excitations that have the same quantum numbers as the low-energy mesons ($\omega,\rho,\ldots$) [15] and they contribute coherently to the renormalization of the single-hole magnetic moments [9,10]. The experimental ground-state magnetic moments, of ^{203,205}Tl, which deviate strongly from the Schmidt value [16], are reproduced by the theory as well as those for ^{207}Pb and ^{209}Bi calculated in [9,10]. The model magnetization distributions are then used to calculate the HFS of hydrogenlike thallium.

Due to the lack of experimental data results are compared to calculated HFS splittings derived in the single-particle approximation. The performed analysis confirms the previously observed trend [9,10] for the thallium hydrogenlike ions. The calculated Bohr-Weisskopf term (ϵ) is larger than that obtained in perturbation theories [11,12,17]. The reason for this systematic disagreement could be the modification of the magnetization and the charge distribution by the additional DCM terms. The electron Dirac spinor is affected by the change of the charge distribution in a similar way as by associating QED corrections to the electron wave function. Thus, some QED corrections could be already included in the DCM.

II. THEORY

A. Mixing of one-hole and dynamic correlations

The DCM ground-state wave functions of the ^{203,205,207}Tl isotopes are formed by coupling the proton hole with collective excitations of the reference core. Generally, a ground-state wave function $|\phi_J\rangle$ of a [A(closed-shell)-1] nucleus has the following form:

$$|\phi_J\rangle=\left[\chi^0_{j_J}a_J+\sum_{j_1j_2j_3J_1}\chi^1_{j_1j_2j_3J_1J}N^1_{j_1j_2j_3J_1J}A_1(j_1(j_2j_3)J_1;J)+\cdots\right]|0\rangle$$
$$=\left[\chi^0_{\alpha_0J}a_J+\sum_{\alpha_1J_1}\chi^1_{\alpha_1J_1J}N^1_{\alpha_1J_1J}A_1(\alpha_1J_1;J)+\cdots\right]|0\rangle, \tag{1}$$

where the operators a_J and $A_1(\alpha_1J_1;J)$ create a single valence-hole and the two-hole one-particle [h-(p-h)] states, respectively. To simplify, we have introduced the notation $\{\alpha_0\}$ for the $\{J\}$ and $\{\alpha_1\}$ for the $\{j_1j_2j_3\}$ quantum numbers. The symbol $|0\rangle$ represents the model vacuum, $\{N\}$ the norm, and $\{\chi\}$ the model amplitudes. The superscript 1 of N and χ, as well as the subscript 1 of A, characterize the excitation of a single particle-hole pair. A diagramatic representation of such a wave function is shown in Fig. 1(a), where the admixture amplitudes are suppressed for simplicity. The thick arrow on the left represents the composite particle, i.e., a particle dressed by one or more particle-hole excitations of the core as given on the right.

The amplitudes of the different modes ($\chi^0_{\alpha_0J}$ and $\chi^1_{\alpha_1J_1J}$) are calculated in the dynamic approximation [8–10]. This method is based on the following commutator equations:

$$[H,A_0(\alpha_0;J)]=\sum_{\alpha_0'}\varepsilon_JA_0(\alpha_0';J)+\sum_{\alpha_1J_1}\langle A_0^\dagger(\alpha_0;J)\|V\|A_1(\alpha_1J_1;J)\rangle A_1(\alpha_1J_1;J), \tag{2}$$

$$[H,A_1(\alpha_1J_1;J)]=\sum_{\alpha_0'}\langle A_1^\dagger(\alpha_1J_1;J)\|V\|A_0(\alpha_0';J)\rangle A_0(\alpha_0';J)$$
$$+\sum_{\alpha_1'J_1'}\langle A_1^\dagger(\alpha_1J_1;J)\|H\|A_1(\alpha_1'J_1';J)\rangle A_1(\alpha_1'J_1';J). \tag{3}$$

In Eqs. (2) and (3) the nuclear Hamiltonian is

$$H=H_0+V=\sum_\alpha\varepsilon_\alpha a^\dagger_\alpha a_\alpha+\frac{1}{2}\sum_{\alpha\beta\gamma\delta}V_{\alpha\beta\gamma\delta}a^\dagger_\alpha a^\dagger_\beta a_\delta a_\gamma,$$

where $V_{\alpha\beta\gamma\delta}$ are the matrix elements of the two-body potential V

$$V_{\alpha\beta\gamma\delta}=\langle\alpha\beta\|V\|\gamma\delta\rangle,$$

and ε_α are the single-particle energies, which can either be obtained by Hartree-Fock calculations or from the low-lying spectrum of neighboring closed-shell nuclei, for this work the latter approach was used. In order to obtain Eqs. (2) and (3), a dynamical linearization procedure [18] for the higher-order components has been used: third-order components are approximated by a sum of second-order terms as illustrated in Fig. 1(b).

The eigenvalue equation for the amplitudes $\chi^0_{\alpha_0J}$ and $\chi^1_{\alpha_1J_1J}$ of the nuclear modes is derived by taking the expectation value of Eqs. (2) and (3) between the vacuum and the states $|\phi_J^{1h+2h1p}\rangle$,

TABLE I. Single-particle scheme used to build the model CMWFs.

Proton hole	$2p_{3/2}$	$1f_{5/2}$	$2p_{1/2}$	$1g_{9/2}$	$2d_{5/2}$	$1g_{7/2}$	$3s_{1/2}$	$2d_{3/2}$	$1h_{11/2}$	
Proton particle	$1h_{9/2}$	$2f_{7/2}$	$3p_{3/2}$	$3p_{1/2}$	$1i_{13/2}$	$3d_{5/2}$	$2g_{7/2}$	$4s_{1/2}$	$3d_{3/2}$	$2h_{11/2}$
Neutron hole	$2d_{5/2}$	$1g_{7/2}$	$3s_{1/2}$	$2d_{3/2}$	$1h_{11/2}$	$1h_{9/2}$	$2f_{7/2}$	$3p_{3/2}$	$2f_{5/2}$	$3p_{1/2}$	$1i_{13/2}$
Neutron particle	$3d_{5/2}$	$2g_{7/2}$	$4s_{1/2}$	$3d_{3/2}$	$2h_{11/2}$	$1j_{15/2}$	$1i_{11/2}$	$2g_{9/2}$		

$$\sum_{\substack{j_1 j_2 j_3 \\ j_1' j_2' j_3'}} \begin{vmatrix} E-\varepsilon_J & V_{Jj_3'j_1'j_2'} \\ V_{j_1 j_2 J j_3} & E-\varepsilon_{j_1}+\varepsilon_{j_2}-\varepsilon_{j_3}+V_{j_1 j_2 j_3 j_1' j_2' j_3'} \end{vmatrix} \begin{vmatrix} \chi^0_{\alpha_0 J} \\ \chi^1_{\alpha_1 J_1 J} \end{vmatrix} = 0. \tag{4}$$

A diagramatic representation of Eq. (4) is shown in Fig. 1(c). On the basis of this figure we will point out the main differences between perturbative approaches and the DCM. Perturbation calculations, usually performed within few particle-hole terms, modify only the structure of the model operator to form an effective operator without enlarging the model space, while the DCM introduces large configuration spaces, which include also higher-order diagrams. Without these higher-order diagrams it would not be possible to convert the commutator chain into an eigenvalue problem. By neglecting the terms marked as ''diagonal'' in Fig. 1(c) the theory would reproduce the diagramatic development of perturbation theory. Furthermore, in the DCM formulation, the Pauli principle acting between the valence and the core particles has been taken into account, while such an effect has not been considered in perturbative theories of open-shell nuclei so far.

Dealing with the magnetic structure of nuclei [19], perturbation theory considers only special diagrams of the form represented in Fig. 1(a), mainly those having the particle and the hole coupled to $J=1$, all others do not contribute. Contrary, DCM three-particle two-hole ($3p$-$2h$) contributions that appear in the ''diagonal'' part of Fig. 1(c), add terms to the wave function that cannot appear in perturbation theories. Thus, the DCM wave functions include particle-hole pairs who couple to J values different from 1. They contribute coherently to the magnetic structure of the nucleus and are therefore important, even though their amplitudes are generally small compared to those of $J=1$ terms. *De facto* we have a collective flow that affects the magnetic structure in the same way as the consideration of meson contributions in perturbation calculations [15].

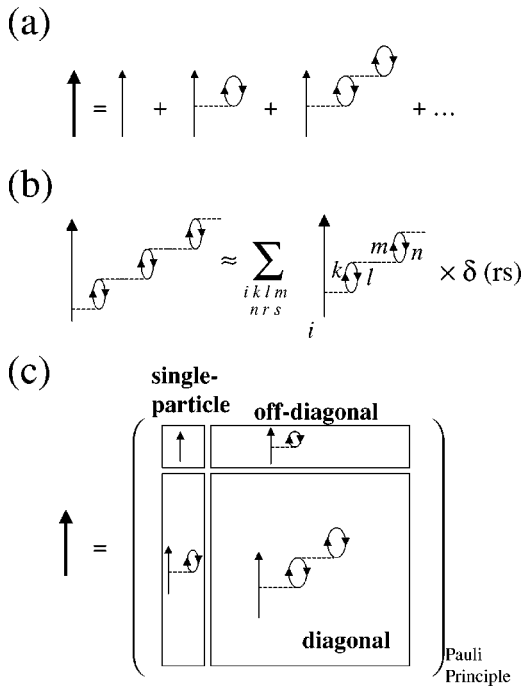

FIG. 1. Dressed particles in the DCM, symbolic representation.

B. Matrix elements of the two-body potential and electromagnetic operators

The matrix elements of the two-body potential appear in Eq. (4) and are thus needed for further calculation of nuclear properties. With some recoupling algebra [20], analytical expressions for these matrix elements can be obtained, which are given explicitly in [10] [Eqs. (2-4) and (2-5)]. They still include the reduced matrix elements of V, which must be calculated numerically. For this calculation a two-body potential of the functional form $V=e^{-(r/b)^2}\Sigma_{S,T}V_{ST}P_{ST}$, where P_{ST} denotes the projection operators onto the two-body states with spin quantum number S and isospin T, has been used. Values for the parameter b as well as V_{ST} for the particle-particle interaction were taken from [21], while V_{ST} for particle-hole interactions was obtained from [22]. This set of parameters has been chosen since they were found to reproduce the low-energy levels of ^{210}Bi and ^{208}Pb in good agreement with experimental spectra. Using harmonic oscillator functions for the single particle, which is necessary since the values for V_{ST} from [21,22] were obtained within this approximation, an analytical expression for the matrix elements can be derived.

The ''dressed'' single-hole states for the Tl isotopes were formed by coupling the $3s_{1/2}^{-1}$ proton hole with all $2h$-$1p$ states up to an unperturbed energy of 30 MeV. The single-particle levels used to form the DCM states are listed in Table I and the single-particle energies of these states were taken from [23], all levels with energies less than $2\hbar\omega$ were considered.

Finally, the mode amplitudes $\chi^0_{\alpha_0 J}$ and $\chi^1_{\alpha_1 J_1 J}$ are determined by numerical diagonalization of Eq. (4). These amplitudes can now be used to calculate electromagnetic properties of the nucleus. For this purpose, the matrix elements of electromagnetic operators O^λ must be evaluated, where O^λ represents either the magnetic moment, the quadrupole moment, or the HFS splitting energy. Again, recoupling algebra allowed us some analytical reduction and the results have

been published previously [10] [Eqs. (2-7)–(2-9)].

We can distinguish between different electromagnetic operators according to the multipole order λ: the magnetic dipole operator does not include any radial dependence, while the quadrupole and HFS splitting operators depend on the radial dependence of the single-particle state. In this case the oscillator wave function, chosen in the calculation of the two-body matrix elements of the nuclear potential is no more justified. Here, a Wood-Saxon potential for the radial dependence of the wave function would be the better choice. Unfortunately, this radial dependence will not allow analytical integration and will, therefore, lead to prohibitively large computing times. In order to obtain an analytical solution, the Wood-Saxon potential can either be expanded in terms of harmonic oscillators or approximated by a single harmonic-oscillator function with the oscillator parameter chosen to reproduce the rms radius. According to [22] the latter approximation has been used.

C. Calculation of hyperfine structure

The energy splitting due to the interaction of the electron with the magnetization of the nucleus is given by

$$\Delta E=\frac{-e\mu_N}{\sqrt{(2F+1)}}\langle[\phi_J\otimes\psi_j^{e^-}]F|(\vec{A}(\vec{r}_e)\cdot\vec{\alpha})|[\phi_J\otimes\psi_j^{e^-}]F\rangle, \tag{5}$$

where we have used the electron current

$$\vec{j}_\mu=-e(\psi_j^{e^-})^\dagger\vec{\alpha}\psi_j^{e^-}, \tag{6}$$

and the vector potential created by the magnetic distribution of the nucleus

$$\vec{A}(\vec{r})=-\int\vec{m}(\vec{r}_j)\times\vec{\nabla}_r\frac{1}{|\vec{r}-\vec{r}_j|}d^3\vec{r}_j, \tag{7}$$

with

$$\vec{m}(\vec{r}_j)=\mu_N\sum_i(g_\ell\vec{\ell}_i+g_s\vec{s}_i)\delta(\vec{r}_j-\vec{r}_i). \tag{8}$$

Here $\vec{\alpha}$ are the Dirac matrices, e is the electron charge, μ_N is the nuclear magneton, g_ℓ and g_s are the orbital and the spin gyromagnetic factors, respectively, J is the nuclear spin, j is the angular momentum of the electron, and F designates the total angular-momentum quantum number of the electron-nucleus system. The ground-state wave functions of the thallium isotopes are given by a superposition of the $3s_{1/2}^{-1}$ hole and the intrinsic core states. According to Eq. (1) they can be written as

$$|\phi_{1/2}^{-1}\rangle=\chi_{1/2}^{\rm sh}|\phi_{1/2}^{-1}\rangle+\chi_{1/2}^{2h1p}|\phi_{1/2}^{2h1p}\rangle, \tag{9}$$

where $\chi_{1/2}^{\rm sh}$ and $\chi_{1/2}^{2h1p}$ are occupation amplitudes given by the following expectation values:

$$\chi_{1/2}^{\rm sh}=\langle 0|a_j^\dagger|\phi_{1/2}^{-1}\rangle\ \text{ and }\ \chi_{1/2}^{2h1p}=\langle 0|a_{j_3}^\dagger a_{j_2}a_{j_1}^\dagger|\phi_{1/2}^{2h1p}\rangle. \tag{10}$$

For the electronic ground state, we solve the Dirac equation for a spherical symmetric (Coulomb) potential of the extended nuclear charge. Two-parameter Fermi-charge distributions with {c,t} parameters of {0.524 fm, 6.59 fm}, {0.524 fm, 6.60 fm}, and {0.524 fm, 6.61 fm} have been used for the nuclear-charge distributions of ^{203,205,207}Tl [11], respectively. For the general case of a magnetization distribution given in terms of angular and spin magnetization we obtain from Eq. (5) the following expression for the energy splitting between the states with total momentum F_1 and F_2:

$$\Delta E=\Delta C(A_L+A_S) \tag{11}$$

with

$$\Delta C=\frac{F(F+1)-J(J+1)-j(j+1)}{2Jj}\Bigg|_{F_1}^{F_2}. \tag{12}$$

The A_L and A_S define the orbital angular momentum and the spin contributions, which are given by

$$A_T=\frac{4}{3}e\mu_N\langle\phi_j|\sum_{\alpha\beta}(\alpha|O_T|\beta)a_\alpha^\dagger a_\beta|\phi_j\rangle, \tag{13}$$

where the operators O_T $\{T=L,S\}$ are

$$O_L=g_\ell\ell_z\left[\int_R^\infty f(r)g(r)dr+\int_0^R\left(\frac{r}{R}\right)^3f(r)g(r)dr\right], \tag{14}$$

$$O_S=g_s s_z\int_R^\infty f(r)g(r)dr-\sqrt{\frac{\pi}{2}}\times[Y_2\otimes\sigma]^1\int_0^R\left(\frac{r}{R}\right)^3f(r)g(r)dr. \tag{15}$$

R is a ''dummy'' variable characterizing the nuclear radial dependence, which is removed in the calculation of the expectation value of A_T. The product $[Y_2\otimes\sigma]^1$ in Eq. (15) denotes the coupling of the spherical harmonic $Y_2(\vartheta,\varphi)$ with the spin operator σ of the nucleon to form a spherical tensor of rank 1; this is the so-called Bohr asymmetry term [24]. The two radial functions, $f(r)$ and $g(r)$, are the large and small components of the electronic wave function in the radial-spherical representation. For ^{203,205,207}Tl with $J=1/2$ we have $\Delta C=4$ and $A_L^{\rm sh}=0$. The following terms contribute to the HFS in the DC model:

$$\Delta E=\Delta E_{\rm sh}+\Delta E_{\text{off-diag}}+\Delta E_{\rm diag}\,. \tag{16}$$

They are given by the expectation values

$$\Delta E_{\rm sh}=\langle\phi_{1/2}^{-1}\psi_{1s1/2}^{e^-}|(\vec{A}(\vec{r}_e)\cdot\vec{\alpha})|\phi_{1/2}^{-1}\psi_{1s1/2}^{e^-}\rangle\chi_{1/2}^{\rm sh}\chi_{1/2}^{\rm sh}, \tag{17}$$

$$\Delta E_{\text{off-diag}}=\langle\phi_{1/2}^{-1}\psi_{1s1/2}^{e^-}|(\vec{A}(\vec{r}_e)\cdot\vec{\alpha})|\phi_{1/2}^{2h1p}\psi_{1s1/2}^{e^-}\rangle\chi_{1/2}^{\rm sh}\chi_{1/2}^{2h1p}, \tag{18}$$

and

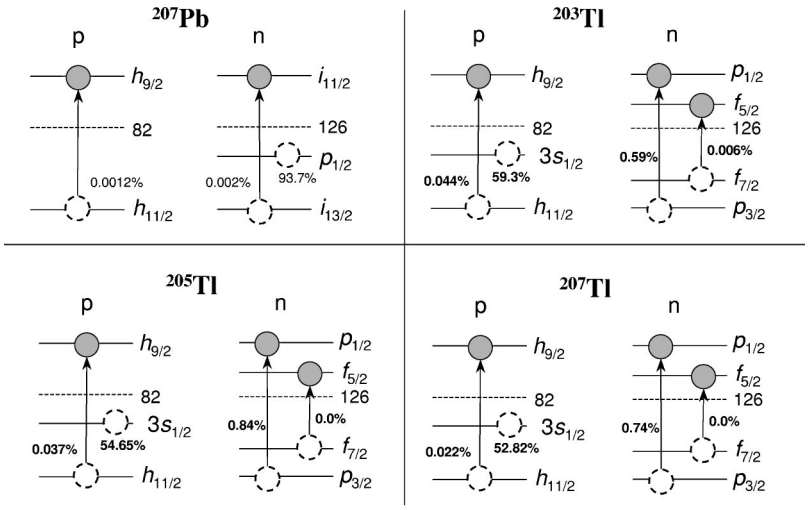

FIG. 2. Single-hole and $J=1$ particle-hole excitations contributing to the dynamic correlations and their admixing coefficients.

$$\Delta E_{\mathrm{diag}}=\langle \phi_{1/2}^{2h1p}\psi_{1s1/2}^{e^-}|(\vec{A}(\vec{r}_e)\cdot\vec{\alpha})|\phi_{1/2}^{2h1p}\psi_{1s1/2}^{e^-}\rangle\chi_{1/2}^{2h1p}\chi_{1/2}^{2h1p}. \tag{19}$$

The single-hole term includes implicitly the Bohr-asymmetry factor, which contributes to the splitting proportional to the single-particle magnetic distribution. The off-diagonal terms take care of the first-order modification generated by an extended nuclear magnetization and correspond to the perturbative diagrams of LeBellac [25]. The DCM-specific correlation terms, leading to ΔE_{diag}, were considered in [9] for the first time. Using this formalism, we calculated the magnetic moment and HFS splittings for the Tl isotopes of interest.

III. RESULTS AND DISCUSSION

A. Nuclear properties

Figure 2 shows the contributions of single-hole and $J=1$ particle-hole excitations to the nuclear ground states of ^{207}Pb and ^{203,205,207}Tl, as obtained from DCM calculations. These are the only spin-flip contributions considered by first-order perturbation calculations. In the case of ^{207}Pb [2] there are three such terms that add up to a total contribution of $\sim$94%. For ^{203}Tl there are four contributing terms due to the larger number of accessible low-energy states for neutron spin-flip transitions (this is not true for ^{205,207}Tl since the $f_{5/2}$ shell is closed and, thus, the $f_{7/2}\rightarrow f_{5/2}$ term cannot contribute to the dynamic excitation mechanism). However, these four (three) terms make up only $\sim$60% of the total nuclear ground-state wave function. The remaining part is correlated with a large number of $J\neq 1$ particle-hole excitations, which are not shown in the figure. The contribution is quite small for each individual term but they all sum up coherently and can change, e.g., the magnetization distribution significantly. This can be clearly seen in Fig. 3, where the magnetization distributions of ^{207}Pb and ^{203,205,207}Tl have been plotted relative to the closed-shell distribution of ^{208}Pb. In each part of the figure, the result for the $3s_{1/2}^{-1}$ hole ($3p_{1/2}^{-1}$ hole for ^{207}Pb) without configuration mixing (occupation amplitude 100%) is given by line *A*, while line *B* represents the same distribution but weighted with the spectroscopic factor given in the corresponding part of Fig. 2. The contribution of particle-hole excitations is represented by line *C* and changes the single-hole distribution considerably; the total magnetization is given by line *D*. The effect is much more pronounced for thallium than for ^{207}Pb and all other nuclei investigated so far.

The mixing coefficients obtained by diagonalization of Eq. (4) were used to calculate the rms radii and the magnetic dipole moments. The results are listed in Table II and are compared to experimentally observed values from [5,26–33]. Additionally we added previously published results [9,10] for ^{165}Ho^{66+}, ^{185,187}Re^{74+}, ^{207}Pb^{81+}, and ^{209}Bi^{82+} to demonstrate the accuracy to which these nuclear properties are reproduced by the DCM. The agreement between theory and experiment is excellent, in most cases within the experimental uncertainty. Only the magnetic moment of ^{207}Tl^{80+} shows a deviation larger than the experimental uncertainty. The reason for this discrepancy is not yet understood; it is not possible for the calculation to reproduce the experimental value using an adjustment of the isotopic parameter that is consistent with the variation adopted for ^{203,205}Tl. In the case

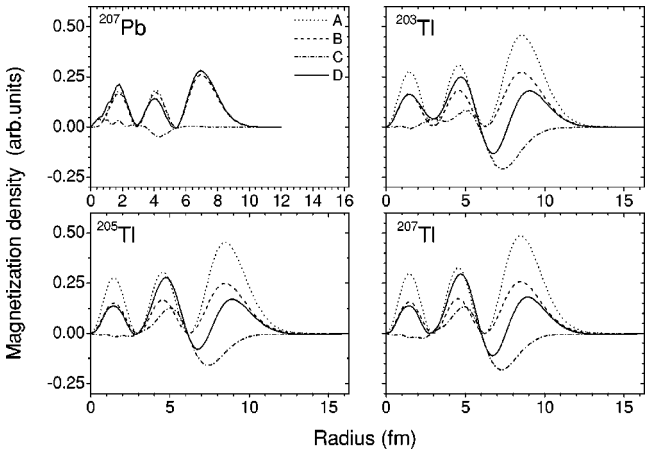

FIG. 3. Calculated magnetization distribution for ^{207}Pb and ^{203,205,207}Tl. Line *A* shows the single-particle result, line *B* has been normalized with the spectroscopic factor of the single particle, line *C* shows the contributions of diagonal and off-diagonal elements in DCM, and line *D* is the total magnetization.

TABLE II. Rms radii and nuclear magnetic moments μ obtained in the dynamic correlation model compared to experimental values. If not explicitly given, the experimental values for the nuclear magnetic moments are taken from [29]. (ABMR, atomic beam magnetic resonance; NMR, nuclear magnetic resonance; CFBLS, collinear fast-beam laser spectroscopy; OP, optical pumping.)

	Nucl. spin J		$\langle r^2\rangle^{1/2}$ (fm)	μ (μ_N)	μ_{Schmidt} (μ_N)	Method
$^{165}Ho^{66+}$	$\frac{7}{2}$	Theory	5.210	4.132	5.793	
		Expt.	5.210 (7) [27]	4.132 (3)		ABMR
$^{185}Re^{74+}$	$\frac{5}{2}$	Theory	5.389	3.1870	4.793	
		Expt.	5.39 (1) [5]	3.1871 (3)		NMR
$^{187}Re^{74+}$	$\frac{5}{2}$	Theory	5.395	3.2196	4.793	
		Expt.	5.39 (1) [5]	3.219 (3)		NMR
$^{203}Tl^{80+}$	$\frac{1}{2}$	Theory	5.469	1.6214	2.793	
		Expt.	5.463 (5) [26]	1.6217 (13)		ABMR
$^{205}Tl^{80+}$	$\frac{1}{2}$	Theory	5.474	1.6379	2.793	
		Expt.	5.470 (5) [26]	1.6372 (2)		ABMR
$^{207}Tl^{80+}$	$\frac{1}{2}$	Theory	5.485	1.6472	2.793	
		Expt.	5.489 (3) [33]	1.876 (5)		CFBLS [30]
$^{207}Pb^{81+}$	$\frac{1}{2}$	Theory	5.496	0.5820	0.638	
		Expt.	5.497 (2) [26]	0.58219 (2)		OP [29,31]
				0.5925 (6)		NMR [28,32]
$^{209}Bi^{82+}$	$\frac{9}{2}$	Theory	5.6	4.110	2.624	
		Expt.	5.519 (4) [26]	4.110 (4)		NMR

of the magnetic moment of $^{207}Pb^{81+}$ the theoretical result shows good agreement with the value obtained by optical pumping [31], which is $\sim 2\%$ smaller than the nuclear magnetic-resonance result [32]. The old value for the rms charge radius of ^{209}Bi has been calculated only to the given accuracy—a meaningful comparison with the experimental result is thus not possible. By comparing the calculated and experimental magnetic moments with the Schmidt values in Table II, one can see that the DCM-induced corrections affect the magnetic moment (and proportionaly the hyperfine splitting) differently for the two spin-flip components ($j = \ell \pm 1/2$), e.g., for ^{203}Tl (proton in $3s_{1/2}$, $j=\ell+1/2$) the correction is $-1.17\mu_N$, while it is $+1.49\mu_N$ in the case of ^{209}Bi (proton in $1h_{9/2}$, $j=\ell-1/2$). Finally, it should be noted that there is an orbital contribution to the magnetic moment of Tl, even though it is an *s*-state nucleus, this is due to the admixture of states with higher angular momentum. It is is important to clarify that we allow $2h$-$1p$ components with either parity, positive and negative. Consequently, the single hole is not necessarily confined to the $3s_{1/2}^{-1}$ state. In the case of ^{203,205,207}Tl the orbital contribution is of the order of 2%, which must be associated to a nonvanishing angular gyromagnetic factor g_ℓ. In other models such a correction of g_ℓ can only be achieved by introducing mesons degrees of freedom in the nuclear system [14].

B. Hyperfine structure

The magnetization distributions shown in Fig. 3 affect the ground-state hyperfine splitting. We listed in Table III the contributions of the different terms defined in Eqs. (17)–(19). The modification due to the off-diagonal and diagonal elements is about 1% of the single-hole contribution throughout all isotopes. The correction relative to the single-hole (single-particle) value is positive for ^{207}Pb and negative for the Tl nuclei for similar reasons as discussed for the magnetic moments. The DCM results for the ground-state hyperfine splitting of thallium isotopes, as well as previously published data for Ho, Re, Pb, and Bi [9,10], are compiled in Table IV. They are compared to splittings calculated for a point nucleus (E_{PN}) and under consideration of the Breit-Schawlow correction for the finite spatial distribution of the nuclear charge (E_{BS}). Additionally, QED radiative corrections [12] are given and combined with the DCM results. Experimental values and results of perturbation calculations are included in the last part of the table. The pure DCM splitting energies agree remarkably well with the experimental values—in all cases the agreement is better than for the perturbative calculations. However, adding the QED contributions leads to a systematic shift and the splittings become too small. Thus it seems that the QED corrections and the DCM calculations are not compatible.

Perturbation approximations assume that the contributions to the HFS arise mainly from the single-particle Bohr-

TABLE III. Single-hole (sh), off-diagonal, and diagonal contributions to the hyperfine structure of various isotopes in the dynamic correlation model. Last column displays the sum. All values are in eV.

	E_{sh}	$\Delta E_{\text{off-diag}}$	ΔE_{diag}	E_{tot}
$^{203}Tl^{80+}$	3.2486	0.0397	−0.0753	3.2130
$^{205}Tl^{80+}$	3.2793	0.0428	−0.0831	3.2390
$^{207}Tl^{80+}$	3.3220	0.0429	−0.0879	3.2770
$^{207}Pb^{81+}$	1.2002	0.0358	−0.0194	1.2166

TABLE IV. Ground-state hyperfine-structure splittings for a point nucleus (E_{PN}), including Breit-Schawlow (E_{BS}), DCM, and QED corrections. The QED contributions include vacuum polarization and self-energy. They were calculated using x_{rad} values from [12] and the experimental magnetic moments listed in Table II. All values are in eV.

	^{165}Ho^{66+}	^{185}Re^{74+}	^{187}Re^{74+}	^{203}Tl^{80+}	^{205}Tl^{80+}	^{207}Tl^{80+}	^{207}Pb^{81+}	^{209}Bi^{82+}
E_{PN}	2.3007	3.0103	3.0411	3.0184	2.9890	2.9716	1.3998	5.8395
E_{BS}	2.1957	2.7976	2.8263	3.3073	3.3374	3.3768	1.2528	5.1922
$E_{\mathrm{tot}}^{\mathrm{DCM}}$	2.1649	2.7192	2.7449	3.2130	3.2390	3.2770	1.2166	5.0832
ΔE_{QED}	−0.0103	−0.0142	−0.0143	−0.0176	−0.0177	−0.0178	−0.0067	−0.0280
E_{tot}	2.1546	2.7050	2.7306	3.1954	3.2213	3.2592	1.2099	5.0552
E_{expt}	2.1646 (6)	2.7187 (18)	2.7449 (18)				1.2159 (2)	5.0841 (4)
Ref.	[4]	[5]	[5]				[2]	[1]

Weisskopf terms and the QED radiative corrections according to

$$\Delta E(\mu)=\frac{4}{3}\alpha(\alpha Z)^3\frac{\mu}{\mu_N}\frac{m}{m_p}\frac{2J+1}{2J}mc^2\{A(\alpha Z)(1-\delta)\times(1-\epsilon)+x_{\mathrm{rad}}\},\tag{20}$$

where α is the fine-structure constant, Z is the nuclear charge, and m is the electron mass. The relativistic correction $A(\alpha Z)$ is obtained from an exact solution of the Dirac equation with a Coulomb potential. The factor $(1-\delta)$ is the Breit-Schawlow and $(1-\epsilon)$ the Bohr-Weisskopf correction [13]. The x_{rad} are QED corrections that have been calculated in Refs. [12,34–38]. In this approximation the nuclear magnetic moment is a well-defined input taken from experimental data. In order to compare our results with those of perturbation theory, we associated the whole DCM correction with the Bohr-Weisskopf effect and calculated the correction factor ϵ according to $\epsilon=1-E_{\mathrm{DCM}}^{\mathrm{tot}}/E_{\mathrm{BS}}$. These are listed in Table V and compared to those from perturbative approaches [11,12,17,38]. Again, a systematic deviation is observed: the ϵ values obtained with the DCM are considerably larger; only for ^{207}Pb the value is smaller, because ^{207}Pb is a nucleus with a valence neutron hole. Reviewing this, one has to keep in mind that the magnetization distributions used to calculate ϵ in perturbation theories are obtained from a single-particle or single-hole model and do not reproduce the experimental magnetic moment.

In the DCM, $\Delta E_{\mathrm{off\text{-}diag}}$ and ΔE_{diag} contribute to the magnetization distribution of the nuclei and without these terms the experimental magnetic moments cannot be obtained. Similar terms should be provided in perturbation theory so that the integration of the modified magnetic distribution yields the experimental magnetic moment. Including these more realistic magnetic distributions in perturbation calculations would modify ϵ given by Eq. (20) as well as radiative corrections, because the magnetic operator is included in the QED calculation.

The size of these additional terms could be estimated by a term-by-term comparison of the DCM with results of perturbation theory including the leading QED diagrams. Unfortunately the large uncertainties of the perturbative results and the difficulty of obtaining a realistic error bar for the DCM values does not allow a meaningful comparison. However, a qualitative comparison can still be done by considering that the DCM is a nonlinear theory and that the nonlinear terms reproduce meson contributions in the nuclear structure. This can be justified using similar arguments as those given in [14], where meson corrections have been introduced. These nonlinear terms can, on the other hand, be associated with a modification of the electron Dirac spinor as illustrated diagramatically in Fig. 4. In the figure we are comparing matrix elements of the magnetic N-body distribution (see Fig. 3) with those for a single-hole distribution. In the first line we assume that the DCM contribution generates vector-meson contributions in the single-hole structure. The relation between the two lines is then due to the decay properties of the ρ meson ($\rho\rightarrow e^+e^-$). Hence, the DCM might already include effects that are considered by redefining the free spinor in QED and the disagreement between E_{tot} and E_{exp} in Table IV could be the result of double counting. The central remaining question is how to quantitatively compare the DCM terms and the radiative corrections of Refs. [12,34–38]. The

TABLE V. Calculated Bohr-Weisskopf terms ϵ in different theories (SO: spin-orbit interaction).

Ref.	^{165}Ho^{66+}	^{185}Re^{74+}	^{187}Re^{74+}	^{203}Tl^{80+}	^{205}Tl^{80+}	^{207}Tl^{80+}	^{207}Pb^{81+}	^{209}Bi^{82+}
[11]	0.0099	0.0118	0.0119	0.0174	0.0174		0.0429	0.0131
[12] (no SO)	0.0085	0.0120		0.0177	0.0177		0.0419	0.0133
[12] (with SO)	0.0089	0.0122		0.0179	0.0179			0.0118
[17]	0.0086	0.013		0.020	0.020		0.036	0.011
[38]								0.0131
DCM	0.0140	0.0280	0.0288	0.0285	0.0295	0.0218	0.0289	0.0210

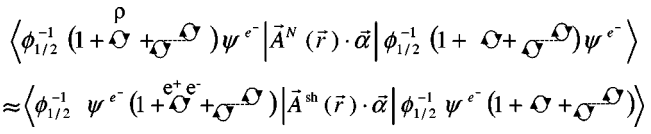

FIG. 4. Diagramatic representation for the connection between higher-order DCM contributions and QED corrections. Considering the decay mode of the vector meson ($\rho \rightarrow e^+e^-$) the DCM correction can be associated with the electron wave function. $\vec{A}^{\rm sh}$ is the vector potential associated with the single-hole magnetic distribution and $\vec{A}^N$ is associated with the many-body magnetization distribution.

importance of this problem is evident. In the extreme single-particle model QED and nuclear-magnetization corrections for high-Z atoms are of the same order of magnitude. Thus, the feasibility of testing the QED corrections depends strongly on the accuracy of the model used to evaluate the nuclear magnetization.

Equation (20) can be modified by considering a more realistic single-particle wave function. In [12] a spin-orbit term was introduced in the Wood-Saxon potential in order to include DCM-specific terms in a single-particle description of the magnetization. Variations of ϵ due to this term were within the given theoretical uncertainty for most of the investigated nuclei. However, adjusting the $\langle \mathbf{L}\cdot\mathbf{S}\rangle$ parameter to reproduce the experimental HFS splitting independently from the QED correction is somehow arbitrary and will make a nonambiguous separation between nuclear and QED contributions impossible. Furthermore the large $\langle \mathbf{L}\cdot\mathbf{S}\rangle$ parameter needed to obtain the experimental hyperfine splitting would not necessarily reproduce excited nuclear spectra as has been shown for ^{207}Pb [39]. Finally, the present investigation on Tl shows that *s*-wave protons can have an orbital contribution to the magnetization distribution, which cannot be associated with the spin-orbit parameter.

In Table VI the expected isotope shift between the Tl isotopes ^{203}Tl and ^{205}Tl is given and compared to other predictions. The DCM result is noticeably smaller than the values given elsewhere [11,12,17].

IV. CONCLUSIONS

In this paper the DCM was applied to calculate the 1*s* hyperfine-structure splitting energies of hydrogenlike ^{203,205,207}Tl ions. The ground-state wave functions were described by a nonperturbative equation of motion, which connects the two-hole one-particle and three-hole two-particle configuration-mixing wave functions to the single proton hole. The model reproduces the experimentally observed magnetic moments and rms radii very well.

TABLE VI. Wavelengths of transitions between the ground-state HFS components in hydrogenlike ^{203,205}Tl^{80+} and predicted wavelength shifts $\Delta\lambda$ between ^{203,205}Tl^{80+} in different theories. All values are in nanometers. In [11] the shift has also been extrapolated from accurate experimental data for neutral Tl. This value has been included in the table (†).

Ref.	^{203}Tl^{80+}	^{205}Tl^{80+}	$\Delta\lambda$ (^{203}Tl^{80+}-^{205}Tl^{80+})
This work	385.89	382.79	3.10
[11]	383.97	380.21	3.76
[12]	384.0	380.2	3.80
[17]	382.2	378.6	3.60
[11]			3.640†

In the DCM three terms contribute to the theoretical hyperfine structure. The first term is due to the single-hole magnetization, the second term was introduced in a perturbative approximation [25], and the third term allows for correlation effects in the nucleus and corresponds to higher-order perturbation diagrams [9]. Taking these three terms into account the calculations accurately reproduce the experimental HFS for ^{165}Ho^{66+}, ^{185,187}Re^{74+}, ^{207}Pb^{81+}, and Bi^{82+}. However, if QED corrections are added a systematic discrepancy to experimental results was found. This is in contrast to the good description of nuclear properties by the dynamic correlation model. In this situation it will be interesting to compare the predicted hyperfine-structure splittings in thallium with obtained experimental results.

Note added. Recently we have learned that the measurement of the hyperfine splitting in hydrogenlike thallium ^{203,205}Tl has been successfully performed [40].

ACKNOWLEDGMENTS

We would like to thank Professor B. Fricke, Professor W. Greiner, Professor H.-J. Kluge, Professor A.-M. Mårtensson-Pendrill, Professor V. M. Shabaev, and Professor G. Soff for fruitful discussions and communications. We would also like to thank Professor P. Beiersdorfer for discussions concerning our preliminary and final results.

[1] I. Klaft *et al.*, Phys. Rev. Lett. **73**, 2425 (1993).
[2] P. Seelig *et al.*, Phys. Rev. Lett. **81**, 4824 (1998).
[3] D. A. Knapp, R. E. Marrs, S. R. Elliott, E. W. Magee, R. Zasadzinski, Nucl. Instrum. Methods Phys. Res. A **334**, 305 (1993).
[4] J. R. Crespo López-Urrutia, P. Beiersdorfer, D. W. Savin, and K. Widmann, Phys. Rev. Lett. **77**, 826 (1996).
[5] J. R. Crespo López-Urrutia, P. Beiersdorfer, K. Widmann, B. B. Birkett, A.-M. Mårtensson-Pendrill, and M. G. H. Gustavsson, Phys. Rev. A **57**, 879 (1998).
[6] Th. Stöhlker *et al.*, Phys. Rev. Lett. **85**, 3109 (2000).
[7] P. Beiersdorfer (private communication).
[8] M. Tomaselli, Phys. Rev. C **37**, 349 (1988); Ann. Phys. (N.Y.) **205**, 362 (1991); Phys. Rev. C **48**, 2290 (1993).
[9] M. Tomaselli, S. M. Schneider, E. Kankeleit, and T. Kühl, Phys. Rev. C **51**, 2989 (1995).
[10] M. Tomaselli, T. Kühl, P. Seelig, C. Holbrow, and E. Kankeleit, Phys. Rev. C **58**, 1524 (1998).
[11] M. G. H. Gustavsson, Chr. Forssén, and A.-M. Mårtensson-Pendrill, Hyperfine Interact. **127**, 347 (2000).

[12] V. M. Shabaev, M. Tomaselli, T. Kühl, A. N. Artemyev, and V. A. Yerokhin, Phys. Rev. A **56**, 252 (1997).
[13] A. Bohr and V. F. Weisskopf, Phys. Rev. **77**, 94 (1950).
[14] B. D. Serot and J. D. Walecka, *Advances in Nuclear Physics* (Plenum, New York, 1987), Vol. 16; R. Bauer, J. Speth, V. Klemt, P. Ring, E. Werner, and T. Yamazaki, Nucl. Phys. A **209**, 535 (1973); T. Fujita and A. Arima, *ibid.* **254**, 513 (1975); C. Mahaux, R. F. Bortignon, R. A. Broglia, and C. H. Dasso, Phys. Rev. **120**, 1 (1985).
[15] I. S. Towner, Prog. Part. Nucl. Phys. **11**, 1991 (1984); T. Ericson and W. Weise, *Pions and Nuclei* (Clarendon, Oxford, 1958).
[16] H. Noya, A. Arima, and H. Horie, Prog. Part. Nucl. Phys. **1**, 41 (1958).
[17] V. M. Shabaev, J. Phys. B **27**, 5825 (1994).
[18] G. E. Brown, *Unified Theory of Nuclear Models* (North-Holland, Amsterdam, 1964).
[19] H. Noya, A. Arima, and H. Horie, Suppl. Prog. Theor. Phys. **8**, 33 (1958).
[20] G. Racah, CERN Report No. **61**, 1961 (unpublished); A. De-Shalit and I. Talmi, *Nuclear Shell Theory* (Academic Press, New York, 1963).
[21] Y. E. Kim and J. O. Rasmussen, Nucl. Phys. **47**, 184 (1963).
[22] V. Gillet, A. M. Green, and E. A. Sanderson, Nucl. Phys. **88**, 321 (1966).
[23] T. T. S. Kuo and G. H. Herling, NRL Report No. 2258, 1971 (unpublished).
[24] A. Bohr, Phys. Rev. **81**, 134 (1951).
[25] M. LeBellac, Nucl. Phys. **40**, 645 (1963).
[26] H. de Vries, C. W. de Jager, and C. de Vriex, At. Data Nucl. Data Tables **36**, 495 (1987).
[27] I. Angeli and M. Csatlos, ATOMKI Kozl. **20**, 1 (1978).
[28] M. G. H. Gustavsson and A.-M. Mårtensson-Pendrill, Phys. Rev. A **58**, 3611 (1998).
[29] P. Raghavan, Nucl. Phys. **42**, 189 (1989).
[30] R. Neugart, H. H. Stroke, S. A. Ahmad, H. T. Duong, H. L. Ravn, and K. Wendt, Phys. Rev. Lett. **55**, 1559 (1985).
[31] H. M. Gibbs and C. M. White, Phys. Rev. **188**, 180 (1969).
[32] O. Lutz and G. Stricker, Phys. Lett. **35A**, 397 (1971).
[33] E. G. Nadjakov, K. P. Marinova, At. Data Nucl. Data Tables **56**, 133 (1994).
[34] S. M. Schneider, J. Schaffner, W. Greiner, and G. Soff, J. Phys. B **26**, L529 (1993).
[35] S. M. Schneider, W. Greiner, and G. Soff, J. Phys. B **26**, L581 (1993).
[36] S. M. Schneider, W. Greiner, and G. Soff, Phys. Rev. A **50**, 118 (1994).
[37] H. Person, S. M. Schneider, G. Soff, W. Greiner, Phys. Rev. Lett. **76**, 1433 (1996).
[38] P. Sunergren, H. Persson, S. Salomonson, S. M. Schneider, I. Lindgren, and G. Soff, Phys. Rev. A **58**, 1055 (1998).
[39] T. Kühl *et al.*, in *Lecture Notes in Physics*, edited by S. G. Karshbenboim and F. S. Pavone (Springer, New York, 2001).
[40] P. Beiersdorfer *et al.*, Phys. Rev. A **64**, 032506 (2001).